

# Photoconductive TiO<sub>2</sub> Dielectrics Prepared by Plasma Spraying

Pavel Ctibor <sup>1,\*</sup>  and Libor Straka <sup>2</sup><sup>1</sup> The Czech Academy of Sciences, Institute of Plasma Physics, Za Slovankou 3, 182 00 Prague, Czech Republic<sup>2</sup> Faculty of Electrical Engineering, Czech Technical University, Technická 2, 166 27 Prague, Czech Republic; libor.straka@fel.cvut.cz

\* Correspondence: ctibor@ipp.cas.cz

**Abstract:** Titanium dioxide coatings (TiO<sub>2</sub>) were sprayed using a water-stabilized plasma gun (WSP) to form robust self-supporting bodies with the character of a ceramic disc capacitor (CDC). Agglomerated nanometric powder was used as feedstock. Argon was applied for powder feeding as well as coating–cooling to minimize the influence of ambient air. Stainless steel was used as a substrate, and the coatings were released after cooling. A more than three-millimeter-thick self-supporting TiO<sub>2</sub> plate was observed using HR-TEM and SEM. Porosity was studied by image analysis on polished sections. Thermal post-treatment on the coating was conducted at a rather low temperature of 500 °C. The results of the subsequent dielectric measurement showed high permittivity, but this was strongly frequency-dependent and accompanied by a progressively decreasing loss tangent. On the other hand, the plasma-sprayed TiO<sub>2</sub> exhibited persistent DC photoconductivity under and after illumination with a standard bulb.

**Keywords:** plasma spraying; ceramic disc capacitor; photo-induced conductivity; thick film

**Citation:** Ctibor, P.; Straka, L.Photoconductive TiO<sub>2</sub> DielectricsPrepared by Plasma Spraying. *Appl.**Sci.* **2024**, *14*, 1714. [https://doi.org/](https://doi.org/10.3390/app14051714)

10.3390/app14051714

Academic Editors: Aleksandra Radtke  
and Adrian Topolski

Received: 25 January 2024

Revised: 6 February 2024

Accepted: 8 February 2024

Published: 20 February 2024



**Copyright:** © 2024 by the authors. Licensee MDPI, Basel, Switzerland. This article is an open access article distributed under the terms and conditions of the Creative Commons Attribution (CC BY) license (<https://creativecommons.org/licenses/by/4.0/>).

## 1. Introduction

Plasma-sprayed coatings are produced by introducing powder particles of feedstock material into a plasma jet, which melts them and propels them towards the substrate. The formation of a coating depends on the interaction between the droplet and the substrate or the previously deposited layers, i.e., spreading of the droplet, the formation of a lamella (called a “splat”), and its solidification. A difference in the degree of splat flattening results in differences in the shape and size distribution of porosity. These factors could also affect bonding between lamellae, which affects the cohesion of the coating markedly. In the case of the WSP system, feeding distance and spray distance can affect most of the above-mentioned features.

Titanium dioxide (titania) is frequently sprayed using plasma torches of various designs [1–5]. The resulting coatings are very often oxygen-deficient. In materials research based on inorganic chemistry, a large amount of effort has gone into studying the Ti-O system, and the promising properties of several oxygen-deficient titanium oxide compounds [6–12] are well known. However, everyone working on the plasma spraying of TiO<sub>2</sub> and materials from the Ti-O system knows that many aspects concerning the spray process remain unsolved. Examples of questions arising in connection with the phenomenon of TiO<sub>2</sub> sensitivity to oxygen loss are as follows:

- How can the plasma spray system be set up to ensure that a Ti<sub>x</sub>O<sub>y</sub> coating (with x and y being exactly known) is obtained from TiO<sub>2</sub> powder?
- Once one has obtained a Ti<sub>x</sub>O<sub>y</sub> coating, how is the responsibility for a change in the addressed property (e.g., electrical resistance) distributed between the phenomena at the (i) lattice level, i.e., plasma-induced oxygen-deficient stoichiometry, and (ii) the macroscopic level, i.e., the specific lamellar character of the sprayed coating with its flat pores and crack network?

- Is there an important difference in the coating's oxygen content when the starting powder is in the rutile or anatase phases of TiO<sub>2</sub>?

All of these questions are also closely associated with the spraying of coatings targeted toward electrical, optical, and photocatalytic studies and applications.

The family of titanium suboxides TiO<sub>x</sub> ( $1.66 < x < 2.00$ ) can be subdivided into several groups [10]. Important intervals of the  $x$  value seem to be 1.93 (or 1.89) to 2.00 and 1.75 to 1.89. Within these intervals, individual compounds exist. At above 1.93 (or 1.89), so-called "higher suboxides" have ordered structures with (132) crystallographic shear planes. Near to  $x = 2.0$ , the (132) crystallographic shear planes are dispersed with varying spacing in the rutile matrix. Due to small differences in the oxygen content of the individual phases, these are difficult to identify. They cannot be segregated in polycrystalline TiO<sub>2</sub> compacts [10], but they can be formed in plasma-sprayed coatings.

The composition range of  $1.75 \leq x \leq 1.89$  is a group in which a homologous series of discrete oxides called "Magneli phases" was originally described [12]. These phases are characterized by crystallographic shear (121) planes. The oxides of the series are built up of slabs of a rutile-type structure—the slabs are of infinite extension in two dimensions and of characteristic finite widths of ( $n$  TiO<sub>6</sub>) octahedra in the third direction [10].

Below  $x = 1.75$ , other individual phases exist, but based on research into plasma composition [13], it is nearly impossible to have these phases in a coating in a pure form. The formation of the Magneli phases from the melt relates to destruction of the shear plane structure. It might be preserved in unmolten particles after the spray process only. Furthermore, the O/Ti ratio in the spray powder can be increased by oxidation (e.g., if spraying is conducted in the atmosphere) and decreased by reduction (e.g., if hydrogen is a plasma gas component).

As the reduction proceeds, a neighboring Ti<sup>4+</sup> may change its charge state to Ti<sup>3+</sup>, and the other electron would become a free-moving charge carrier. The ivory-yellow-white color of the fully stoichiometric version turns into a progressively darker blue-gray-black color of a heavily anion-depleted Ti-O sample. The color change is caused by the absorption of red light (photons with energy below the band gap [14,15]) by the conduction electron [11].

Titanium oxides with temperature-stable and environmentally stable dielectric properties characterized by high relative permittivity and low dielectric loss have recently attracted attention due to their impact on the fabrication of novel microelectronic devices and microwave communication systems [16]. Titanium dioxide coatings are widely used in various applications, such as photo-catalysis, bone implants, electric devices, renewable energy systems' components, and gas sensors [1]. Taking this into account, a gradual transition of TiO<sub>2</sub> coating materials from protective surfaces to active functional components has been welcomed and promoted by the whole thermal spray industry.

The plasma spraying of TiO<sub>2</sub> using gas-stabilized plasma systems is well governed [1, 13–16]. In addition to the high cooling rate, low heat transfer to the spray powder, resulting from low hydrogen content and low plasma power, increases the content of anatase in Ar/H<sub>2</sub> plasma-sprayed coatings [10]. Coatings deposited at a higher temperature are characterized by reduced porosity and increased density [17]. In the case of TiO<sub>2</sub>, the anatase-to-rutile phase transition is observed to occur between 500 °C and 900 °C, with the exact temperature being a sensitive function of sample preparation conditions [18,19].

At the Institute of Plasma Physics ASCR (IPP), plenty of various spray parameters have been tested to produce TiO<sub>2</sub> coatings from a conventional crushed [18] powder as well as agglomerated nano-powder [5], and various properties of the coatings have been studied.

Plasma spraying belongs to the well-established branch of thermal spraying. It has been proved that water-stabilized plasma (WSP) spraying is a complementary and useful method of thermal spraying. Plasma units based on this principle produced in the Czech Republic have been successfully applied in several countries in Europe, the USA, and Japan. High energy density and high temperatures result in a very high throughput, in some cases being one order of magnitude higher than that of gas-stabilized systems. Therefore, the

best use of WSP is for large-area coatings, for the production of self-supporting ceramic parts, and for powder processing.

Water-stabilized plasma exhibits substantially different plasma properties in comparison to common gas-stabilized torches and, thus, provides unique capabilities in technological applications. The WSP torch is based on a vortex-stabilized atmospheric DC arc. Water, injected tangentially into the arc chamber, creates a vortex that confines the arc to the center of the chamber. The arc burns between a rod cathode and a rotating copper disc anode, which is placed outside the main body in front of the exit nozzle. The cathode is either a consumable graphite rod or a copper rod with a zirconium tip. Both the anode and the cathode are cooled by water. Continuous evaporation of water walls inside the arc chamber leads to overpressure, which accelerates the plasma (consisting of substances produced due to heating, dissociation, and ionization of steam) towards the exit nozzle, and the plasma jet is injected rapidly into a stagnant environmental atmosphere. The sprayed material is introduced into the plasma jet by one or more external feeders. The feeding gas can be compressed air or an inert gas.

Rutile  $\text{TiO}_2$  melts at 1912 °C and subsequently dissociates to the liquid Magneli-phase compositions  $\text{Ti}_4\text{O}_7$  and  $\text{Ti}_3\text{O}_5$ . The first evaporation product is initially  $\text{TiO}_2$ , but it dissociates at a higher temperature (about 2700 °C) to  $\text{TiO} + \text{O}$  and, finally (at about 3200 °C), to  $\text{Ti} + \text{O}$  [13]. The maximum particle temperature achieved in the WSP process for argon-rich conditions was only 2100 °C [20]. The average particle temperature required to dissociate  $\text{TiO}_2$  into  $\text{TiO} + \text{O}$  and  $\text{Ti} + \text{O}$  (i.e., close to 3200 °C) is certainly not reached at the WSP spraying. The addition of  $\text{H}_2$  into the plasma shifts the onset temperature of all dissociation and decomposition events to significantly lower values [13].  $\text{Ti}_3\text{O}_5$  is formed slightly above 2100 °C. However, atomic hydrogen starts to prevail over molecular hydrogen at about 3000 °C [13]. For the gas-stabilized plasma, one could consider that the hydrogen effect on  $\text{TiO}_2$  is twofold, not only reducing the necessary temperature for the onset of dissociation but also increasing the particle temperature drastically. Therefore, a more reduced  $\text{TiO}_{2-x}$  coating for Ar- $\text{H}_2$  spraying conditions can be expected.

Our WSP plasma initially contains  $\text{H}_2\text{O}$ , later  $\text{H}_2$ , and even later H. In the investigation, argon was added as a powder feeding gas to partly eliminate the reductive capability of hydrogen. The purpose of the work presented here is to investigate the dielectric properties of  $\text{TiO}_2$  produced by Ar-assisted WSP spraying. In the as-sprayed state, the plasma-deposited material cannot be tested as dielectric because of its too-conductive form caused by the oxygen-deficient character [15,17,21]. That is why the thermal annealing process was carried out; however, the annealing regime was very mild so as not to rearrange the microstructure. The novelty of this work is mainly in mapping the response of the electrical charge to light. The light-induced charge is manifested in the phenomena measurable by the resistivity/conductivity and the current flow measurements. The  $\text{TiO}_2$  coating, or the self-standing body resulting from this processing, could be a prospective material for capacitor or sensor applications.

## 2. Experimental Section

### 2.1. Feedstock Powder and Spray Process

$\text{TiO}_2$  powder (Altair Nanomaterials Inc., Reno, NV, USA) was purchased as prepared from a nanometric powder, Figure 1, by agglomeration into so-called “thermal-spray-grade powder”, Figure 2. The producer declared the mean size of initial nanoparticles as 20 nm. The agglomerated particles were globular, and some of them exhibited open or closed central voids. Sometimes, this sort of powder is also called HOSP—hollow sphere powder. The fraction from 45 to 150  $\mu\text{m}$  in size was utilized for the spray experiments at various processing conditions. The samples were produced using the WSP 500 spray system (CAS, Institute of Plasma Physics, Prague, Czech Republic). The powder was fed in through two injectors, and the thickness of the sprayed coatings was about 3 mm. Stainless-steel coupons were used as substrate, and the majority of coatings was subsequently stripped-off for further characterization. Spray parameters, Table 1, were fixed. Argon was used as

a powder feeding gas, with a pressure of 2.5 bar and a flow rate of 3.25 slpm employed. Argon was also used for substrate cooling and cooling the just-deposited coating. The cooling tube was installed on a robotic arm, and after each pass, it copied the movement pattern of the spray gun over the substrate. The temperature was monitored by a two-color pyrometer not to exceed 250 °C. The torch is shown schematically in Figure 3a. The plasma jet exists along the whole spray distance (SD). The spray process photography is depicted in Figure 3b. Individual splats were collected on mirror-polished stainless steel to check their desirable circular character, Figure 4.

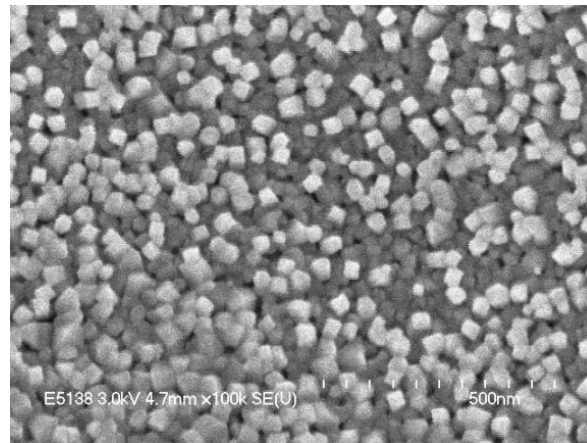


**Figure 1.** Initial TiO<sub>2</sub> nanoparticles, SEM-SE (scale bar 500 nm).

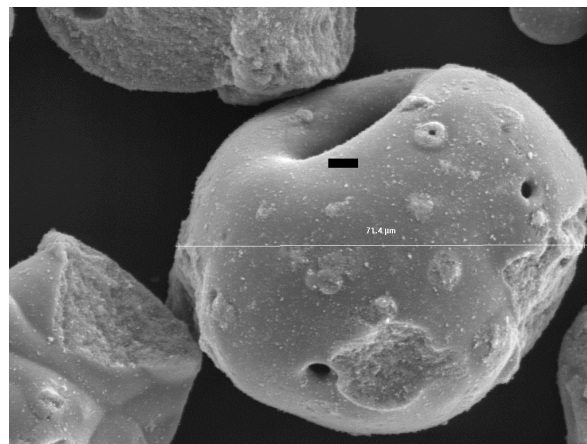
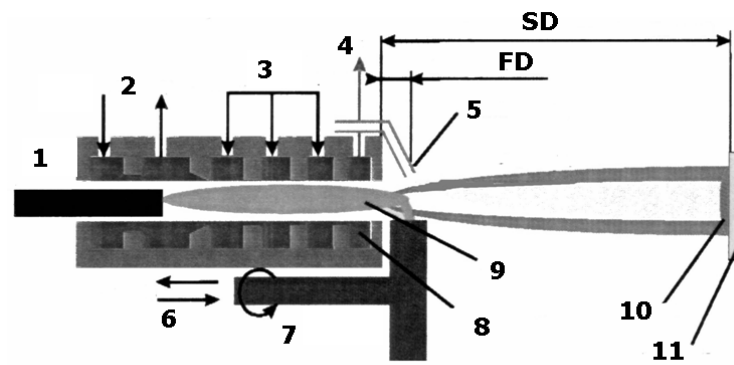


**Figure 2.** Agglomerated TiO<sub>2</sub> thermal-spray-grade powder, SEM-SE (shown particle diameter 71.4 μm).

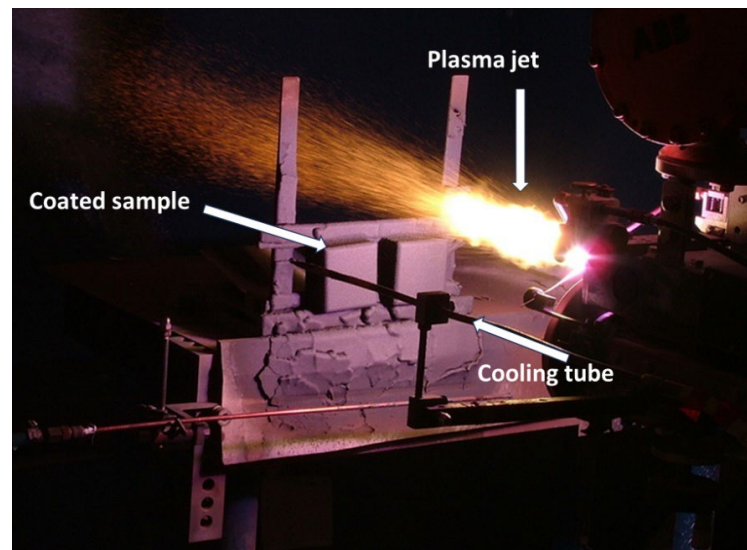
**Table 1.** Parameters used for spraying.

Parameter	Value
Feeding distance FD [mm]	120
Spray distance SD [mm]	400
Feeding nozzle diameter [mm]	3
Torch power [kW]	150

Annealing of the plasma-sprayed deposits was carried out on the samples released from the metallic substrate (self-supporting bodies) in a laboratory furnace in air atmosphere. The heating and cooling ramps were 7 °C per minute, and the dwell time at the maximum temperature was 30 min. The annealing temperature (500 °C) was selected with respect to re-oxidation of the as-sprayed titania coatings, usually oxygen-deficient [6–12], which, according to our preliminary tests, starts at around 500 °C.



(a)



(b)

**Figure 3.** (a) Scheme of spraying with WSP. 1—cathode; 2—cathode cooling water in and out; 3—plasma stabilization by water; 4—water outlet; 5—powder feeding tube; 6—anode cooling water in and out; 7—anode rotation; 8—water vortex; 9—electric arc; 10—coating; 11—substrate; FD—feeding distance; SD—spray distance. (b) WSP spray setup at work.

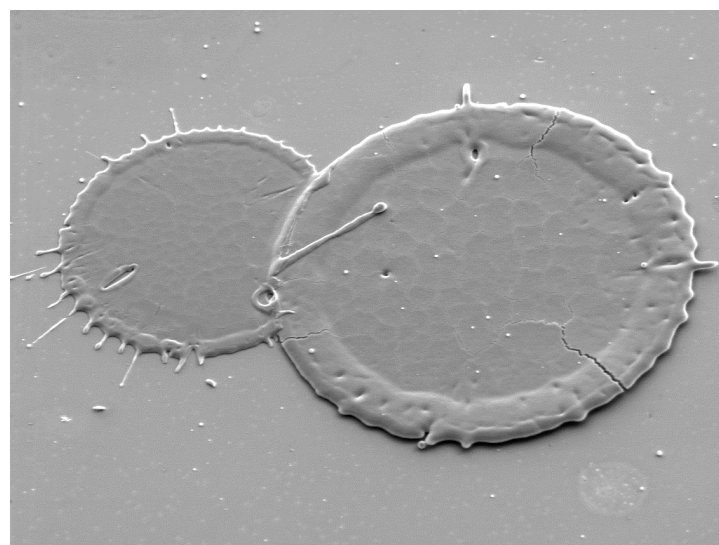


**Figure 4.** Two solidified droplets (splats) on a polished surface, SEM-SE, 270× magnification.

## 2.2. Characterization Techniques

### 2.2.1. Microstructure

Microstructure of the coatings was studied by a High-Resolution Transmission Electron Microscope (HR-TEM) Jeol JEM 3010 (Jeol, Eindhoven, The Netherlands). Surface of the splats and coatings was observed using Scanning Electron Microscopy (SEM) using EVO MA 15 (Carl Zeiss SMT, Oberkochen, Germany) in the secondary electrons (SE) detection mode.

### 2.2.2. Dielectric Parameters

If a difference in electric potential is applied across the plates of a capacitor, an amount of charge will be stored between the parallel plates. This increase is proportional to the relative permittivity of the material used, which is dependent on the degree of polarization or charge displacement in the material. Capacitance describes the ability of a material to concentrate electrostatic flux within the spatial volume that the material occupies. Capacitance recalculated according to the dimensions of the dielectric layer gives the relative permittivity (called also “dielectric constant”).

The dielectric parameters of plasma-sprayed TiO<sub>2</sub> were measured on a square sample with a circular measurement electrode, forming a ceramic disc capacitor (CDC). Before the metallization, the sample was ground with the SiC paper to eliminate surface unevenness. Using a mask, a three-electrode system was applied to diminish the stray-current effect during measurement. The bottom face was fully covered with sputtered aluminum. The top face was sputtered to form an internal circle electrode, 16 mm in diameter, and an external ring electrode (earth-connected during the measurements) separated from the internal ring with a 1 mm wide gap.

Electric field was applied along the spraying direction (i.e., through the thickness). Capacitance of the samples was measured using a programmable impedance analyzer model 4284A (Agilent, Santa Clara, CA, USA), while the sample was clamped using a high-precision sample fixture 16451B (Agilent, Santa Clara, CA, USA).

The dielectric constant (i.e., relative permittivity) was calculated according to Equation (1),

$$\epsilon_r = C \times d / \epsilon_0 \times A \quad (1)$$

where  $\epsilon_r$  is relative permittivity,  $C$  (F) is equivalent parallel capacitance obtained from the measurement,  $d$  (m) is sample thickness,  $A$  is surface electrode area of the internal circle, and  $\epsilon_0$  is permittivity of vacuum ( $8.85 \times 10^{-12}$  F/m).

Thermal coefficient of capacitance (TCC) describes thermal stability of capacitance (and permittivity) when the dielectric measurement is carried out at two temperatures with a difference at least 100 °C. A low value of TCC is desirable to make the circuit component, based on the studied material, work well during the unavoidable thermal fluctuations. TCC is expressed in ppm/°C, and in our case, it was calculated using the capacitance measured at 30 °C and 140 °C.

When a sinusoidal alternating voltage is applied to an ideal capacitor, the current advances by  $\pi/2$  in phase. In the case of a practical capacitor, however, the advance in phase is  $(\pi/2 - \delta)$ , which is smaller than  $\pi/2$ . The angle  $\delta$  is referred to as loss angle and its tangent function as loss tangent. The loss tangent (or “dissipation factor”) is numerically equal to the ratio of the active dissipative current to the reactive (charging) current. The dielectric loss of TiO<sub>2</sub>, obtained in the form of the loss tangent  $\tan \delta$ , was measured simultaneously with the relative permittivity. Measurements at elevated temperatures were carried out using a programmable furnace Novotherm (Novocontrol, Montabaur, Germany) equipped with a special Broadband Dielectric Spectroscopy (BDS) sample fixture 1200 (Novocontrol, Montabaur, Germany).

The DC volume resistance was measured on the same sample as capacitance using a Keithley 6517-B (Keithley Instruments, Solon, OH, USA) programmable resistometer. The applied voltage was  $50 \pm 0.2$  V. Customized Keithley 6104 shielded test enclosure was used

to avoid errors from any external noise. Resistivity  $\rho$  was calculated from the measured resistance and specimen dimensions using Equation (2),

$$\rho = (R \cdot A) / d \quad (2)$$

where  $R$  ( $\Omega$ ) is sample electrical resistance,  $A$  ( $m^2$ ) is area of the internal circle electrode, and  $d$  (m) is sample thickness.

### 2.2.3. Electrical Response to Visible Light

Photoconductivity is divided into two categories [22]: (i) persistent photoconductivity (PPC) and (ii) transient photoconductivity (TPC). The PPC phenomenon is an electrical conductivity enhancement when the material absorbs electromagnetic radiation (light), and the enhancement in conductivity remains for a considerably long time even after the removal of the light source. On the other hand, in the case of TPC, the material regains its initial conductivity as soon as the light source is removed.

The photoconductivity of the  $TiO_2$  sample was tested using a standard 60 W bulb during the simultaneous measurement of electrical DC resistance. Light power of  $20 \text{ mW} \times \text{cm}^{-2}$  was used, and DC bias was set to 50 V. Resistance values were recorded every 30 s. About 23 mW of radiation power impacted the naked surface of  $TiO_2$ . A graph showing volt-ampere characteristics (VAC) was created using voltage sweep from 0 to 100 V DC, with a step of 5 V and a time step of 10 s. The current is shown in microamperes.

## 3. Results and Discussion

### 3.1. Microstructure and Porosity

The coating was formed mainly by smooth circular splats, Figure 4, which is a near-optimum character of the coating building blocks. However, when those blocks were stacked to make a thick coating, various imperfections accumulated and formed cracks, pores, and non-well-flattened particles or particle clusters. An example of such a structure, typical for plasma-sprayed ceramics, is shown in Figure 5. The as-sprayed porosity, Table 2, can be characterized not only with its area fraction on the cross-section ("porosity") but also with its size ("ED", equivalent diameter) and count ("pores per  $\text{mm}^2$ "). High porosity with a low count indicates large pores (confirmable with high ED as well), and oppositely, a high quantity of pores per area unit in combination with low porosity would signal very fine pores. The limit of such quantification, used in Table 2, is around  $3 \mu\text{m}$ , and finer pores are not counted reliably. The shape criterion used here is the minimal circularity (CIR). Globular pores have a cross-section circularity value one, whereas very flat pores approach zero. "CIR<sub>min</sub>" is the minimum CIR value for the field of view, i.e., detection of an extremely flat void. The image analysis values for the as-sprayed  $TiO_2$  (labeled n- $TiO_2$  as "nano") should be shown in relations with similar coatings to provide an idea if, for example, ED  $13.55 \mu\text{m}$  is a large value or not. For this reason, another two coatings sprayed by the same team and evaluated with the same approach were added in Table 2.

**Table 2.** Image analysis of pores in the coatings.

Sample	Porosity [%]	ED [ $\mu\text{m}$ ]	Pores Per $\text{mm}^2$	CIR <sub>min</sub>
n- $TiO_2$ *	$8.53 \pm 1.93$	$13.55 \pm 1.17$	$171 \pm 68$	$0.095 \pm 0.026$
$TiO_2$ **	$4.60 \pm 0.90$	$9.00 \pm 0.50$	$389 \pm 57$	$0.030 \pm 0.010$
$TiO_2$ ***	$3.33 \pm 0.55$	$5.45 \pm 0.49$	$363 \pm 56$	$0.105 \pm 0.028$

\* the actual research; \*\*  $TiO_2$  sprayed from fused and crushed natural rutile  $TiO_2$  [18]; \*\*\*  $TiO_2$  sprayed from Metco 6232B commercial powder with a gas-stabilized plasma torch [21].

A comparison of the samples (Table 2) showed n- $TiO_2$  to be rather porous, with a large ED and a low count, whereas the CIR<sub>min</sub> parameter was medium, rather high in fact, since the gas-stabilized plasma torches produced a typically finer microstructure,

with finer, and also on average flatter, voids. There would be room for microstructure improvements in the n-TiO<sub>2</sub> coating via some post-processing as post-HIP (hot isostatic pressing), laser re-melting or simply long-time high-temperature annealing. Often, the microstructure obtained applying this post-processing approaches the one typical for sintering. However, our annealing was only very mild to restore the coating stoichiometry to the extent to behave dielectrically only (not like a conductor, which an oxygen-deficient titania could [10,15]) and, on the other hand, not to affect the microstructure with crack healing, pore coagulation, or similar effects.

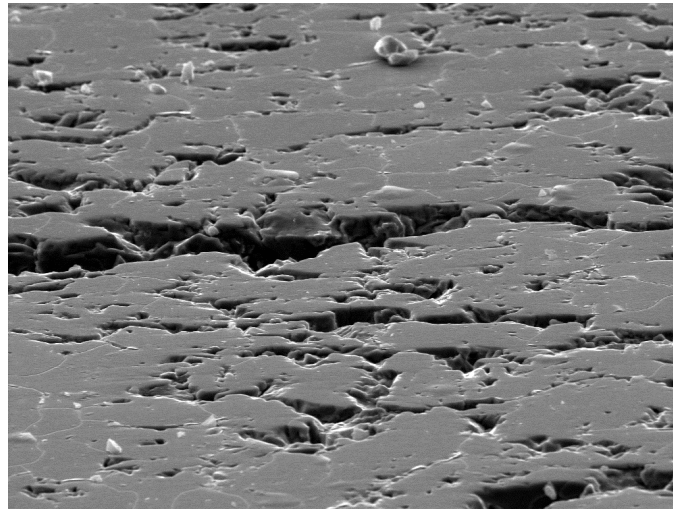


**Figure 5.** Coating's polished surface, SEM-SE—500× magnification, tilt 75°.

The HR-TEM image, Figure 6, shows at least one kind of defect that can often be observed—dislocations. The extra atom plane of the dislocations can be found by viewing along the direction indicated by the arrows seen in the figure. This dislocation should have an edge component, since there is an extra plane of atoms. It has been noted that this type of dislocation is more often observed in the region in which a strong lattice strain exists [23].

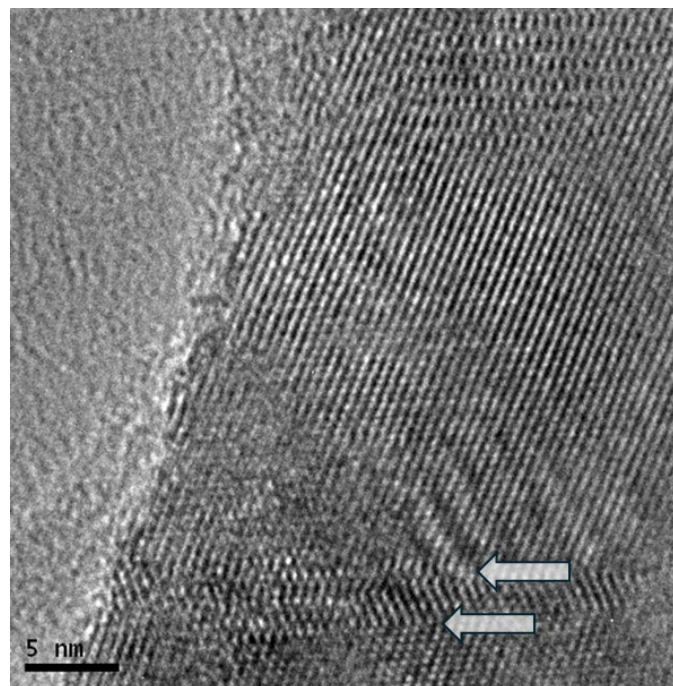


**Figure 6.** HR-TEM of the n-TiO<sub>2</sub>, scale bar 5 nm.

### 3.2. Dielectric Behavior

The relative permittivity of the n-TiO<sub>2</sub> sample, Figure 7, at room temperature (R.T.) started at 160 Hz with the value of 34, which is lower than the literature-based dielectric constant of polycrystalline TiO<sub>2</sub> (55 to 89 [24]). With growing frequency, the permittivity decreased, with a final value of 9.3 at a frequency 28 MHz. This drop was because of structural imperfections inherently present in plasma-sprayed coatings (pores, micro-cracks, local deviations from stoichiometry). With the increasing measurement temperature, the permittivity rose. The difference at low frequencies is huge, and at a high frequency, the values converge toward a unified magnitude of ~10. The difference at 160 Hz was 34 for R.T. versus 2100 for 250 °C, whereas the difference at 28 MHz was 9.3 for R.T. versus 10.8 for 250 °C. This is in full concordance with the polarization mechanisms taking place at various frequencies. The interfacial or space charge polarization produces considerably large relative permittivity only at low frequencies. If the frequency rises, the dipolar polarization subsequently ceases. The ionic polarization was also active in the MHz range, but this was the same for all the temperatures applied, since the compound is a simple oxide with no dopants. Due to these physical aspects, the run of permittivity, as in Figure 7, is expectable.

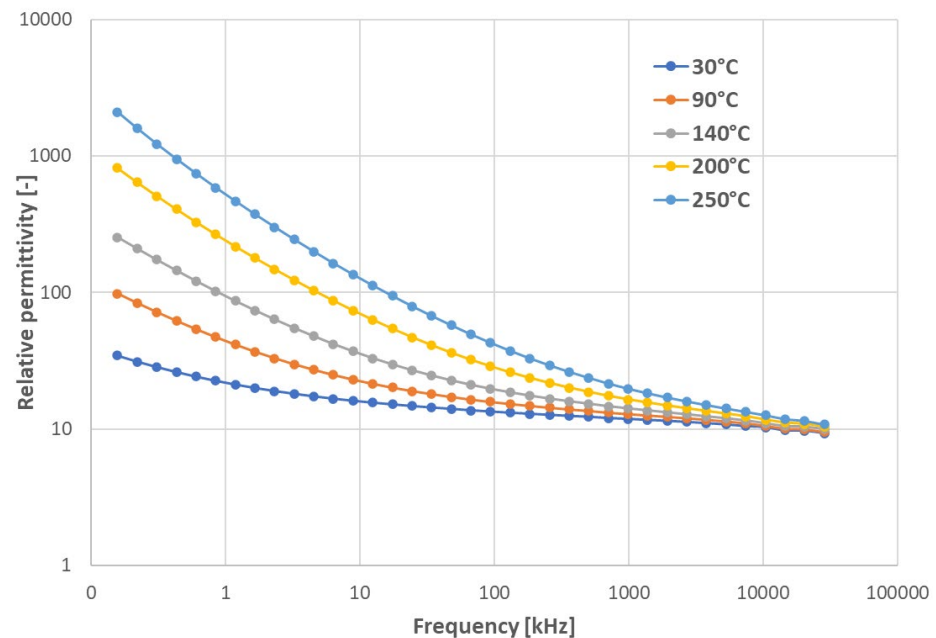


**Figure 7.** Relative permittivity of plasma-sprayed n-TiO<sub>2</sub>.

The loss tangent, Figure 8, dropped with the growing frequency as well. At R.T., its values ranged between 0.8 and 0.08. For the highest measured temperature 250 °C, it was between 5.0 and 0.3. Over 100 °C, the decrease was monotonous, whereas up to 100 °C, a local peak around 8 MHz existed. The existence of two separable components of losses could be recognized [25]. The high-frequency component was one, where  $\epsilon''_r$  corresponded to the part of the losses associated with the relaxation phenomena (cf. the semicircular halo in Figure 8 with maxima above 8 MHz). The low-frequency component exists due to a purely conductive mechanism. However, compared to several materials produced by electric-field-assisted sintering [26], the conductivity due to free charges is much less pronounced, and such a loss component is more due to the interfacial polarization.

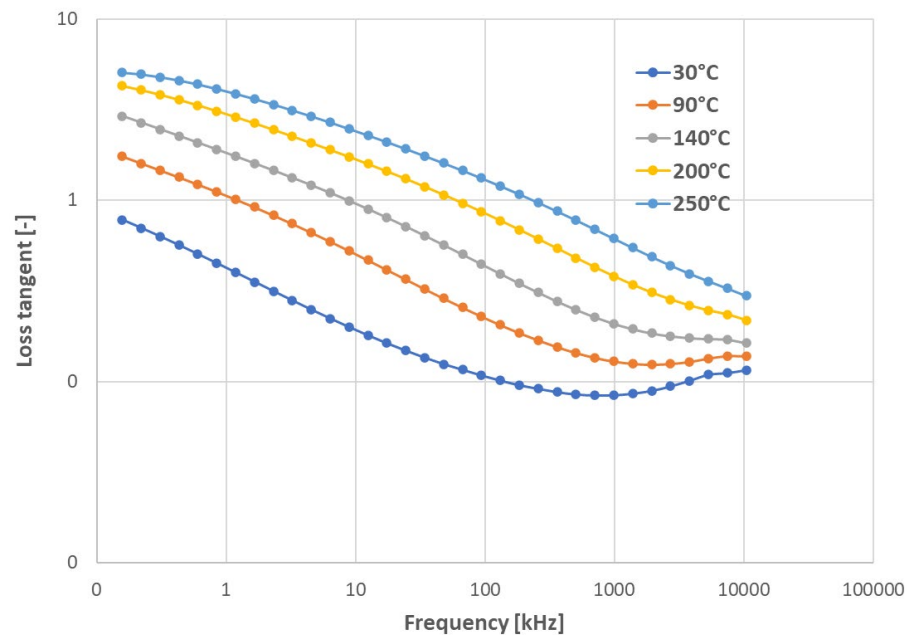


**Figure 8.** Loss tangent of plasma-sprayed n-TiO<sub>2</sub>.

The thermal coefficient of capacitance (TCC) value was 643 ppm/°C. A value of about 400 ppm/°C is typical for sintered TiO<sub>2</sub> [27]. If the plasma deposit microstructure with pores and cracks is considered, the measured value could be accepted as rather good, however, open to further optimization.

### 3.3. Photoconductivity

Run of the volume DC resistivity was observed in time, Figure 9. Light was first switched on after 3.0 h and switched off after 6.2 h after the beginning of the experiment. We saw a rather fast decrease in resistivity under illumination, which was later saturated. This corresponds to the activation of charge carriers and their subsequent depletion. Photoconductivity at room temperature could be mostly ascribed to the increment in carrier density under illumination. The new “stable” value induced by light was at about 20 MΩm, i.e., a decrease to about 42.5% of the initial value (i.e., the value before enlightenment being considered 100%). After switching the light off, the recovery started. In our experiment, this process was similarly fast as the decay (approximately 3.2 h). This interval can be called a persistent photoconductivity period. The initial horizontal trend of the “dark” resistivity was followed further. The experiment showed a relatively large, but slow, fully recoverable photo-induced change in resistivity (or, inversely, conductivity). In principle, similar transient photo-current responses have been detected at electrochemical measurements by other authors [25]. High and persistent photoconductivity of an oxide hetero-structure has been described [22] but for a system consisting of a thin LaFeO<sub>3</sub> film grown on a SrTiO<sub>3</sub> single crystal. The reproducibility of the photoconductivity phenomenon was monitored, Figure 9, for a total duration of 45 h. The “light-off” periods were characterized by a resistivity mean value  $32.83 \pm 0.73$  MΩm, and the “light-on” periods by a resistivity mean value  $19.46 \pm 0.12$  MΩm. The narrow “secondary” peaks, indicated in the figure by arrows, present because of fluctuations (various source instabilities and ripples), were abandoned for the calculations.

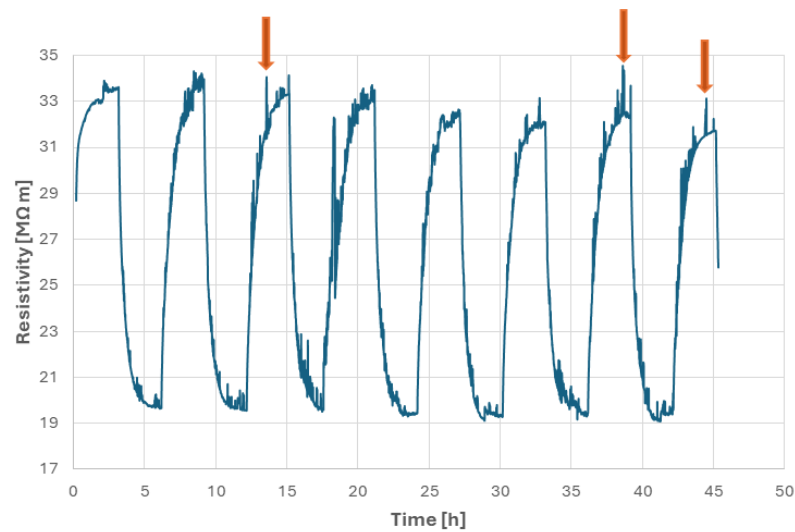


**Figure 9.** Photoconductivity (expressed as resistivity variation in time).

The same coating, but annealed at 750 °C, had a stationary (“dark”) resistivity value of about 1300 MΩm, as published earlier [20]. The higher the annealing temperature, the stronger the re-oxidation back to the exact TiO<sub>2</sub> form, and the higher the “dark” resistivity. Material CaCu<sub>3</sub>Ti<sub>4</sub>O<sub>12</sub> (CCTO) was exposed to 200 mW × cm<sup>-2</sup> (i.e., 10-times higher than in our case) of light with the intensity maximum at 405 nm (i.e., violet, whereas our light was much closer to red) [28]. Upon violet light exposure, the CCTO resistance showed an initial rapid decrease ascribed to oxygen-vacancy states induced by the light [28].

The DC volt-ampere characteristics (VAC) of an n-TiO<sub>2</sub> sample were recorded, Figure 10. The signal was received at sweep from 0 V to 100 V DC, with a voltage step of 5 V and a time step of 10 s. Two dependencies are shown—VAC for the dark conditions (label “off”), and VAC recorded after turning the light on (label “on”). The graph shows that the stronger the voltage, the more pronounced the light-induced photo-conductance. This phenomenon is strictly linear for voltages over 20 V. The value of about 15 V represents a threshold value, under which the current flow is negligible. This character would be prospective for the sensor function of the n-TiO<sub>2</sub> coating.

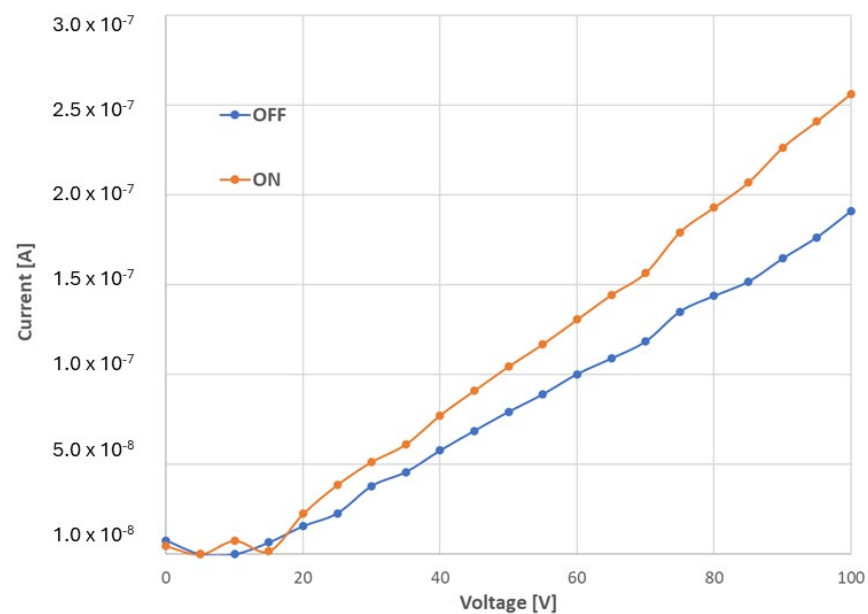


**Figure 10.** Volt-ampere characteristics (VAC) of the n-TiO<sub>2</sub> coating.

#### 4. Conclusions

Titanium dioxide commercial powder formed from nanoparticles using agglomeration was plasma sprayed. The thick coatings were stripped off the substrate to form self-supporting bodies with a ceramic disc capacitor character. In addition to the microstructure investigation, such a body was subjected to mild annealing. In the as-sprayed state, the plasma-deposited material cannot be tested as a dielectric because of its too-conductive form due to the oxygen-deficient character [15,17,21]. After very mild thermal annealing, the sprayed disc could be tested as a dielectric and as a photoconductive material. The character of the dielectric response was like “colossal permittivity ceramics”, i.e., a steep drop of permittivity from quite a high value to medium values with increasing frequency. The lossy character of the ceramics was, however, not as pronounced as for several sintered colossal permittivity ceramics. The photo-activated change in DC resistivity, using visible light and constant voltage bias, was rather strong (42%) and persistent for a couple of hours. The volt-ampere characteristics were modified by visible light conditioning as well. This material has prospects for sensor applications. Since plasma spraying is capable of covering large areas of substrates with variously thick coatings [29,30], including curved surfaces, and due to the capability of this process to produce useful sensors including functionally graded ones, or other particular arrangements, we consider the demonstrated functionalities of plasma-sprayed TiO<sub>2</sub> to be very promising.

**Author Contributions:** Conceptualization, P.C.; methodology, P.C.; software, L.S.; investigation, L.S. and P.C.; data curation P.C. and L.S.; writing—original draft preparation, P.C.; writing—review and editing, P.C. All authors have read and agreed to the published version of the manuscript.

**Funding:** This research received no external funding.

**Institutional Review Board Statement:** Not applicable.

**Informed Consent Statement:** Not applicable.

**Data Availability Statement:** The data for the elaboration of this manuscript are non-public. They are stored by the authors and will be available to readers upon email request, ctibor@ipp.cas.cz.

**Acknowledgments:** Our coworkers from all auto-cited references in this article.

**Conflicts of Interest:** The authors declare no conflicts of interest.

#### References

1. Gardon, M.; Guilemany, J.M. Milestones in Functional Titanium Dioxide Thermal Spray Coatings: A Review. *J. Therm. Spray Technol.* **2014**, *23*, 577–595. [[CrossRef](#)]
2. Sharma, A.; Gouldstone; Sampath, S.; Gambino, R.J. Anisotropic Electrical Conduction from Heterogeneous Oxidation States in Plasma Sprayed TiO<sub>2</sub> Coatings. *J. Appl. Phys.* **2006**, *100*, 114906. [[CrossRef](#)]
3. Bordes, M.C.; Vicent, M.; Moreno, R.; García-Montaño, J.; Serra, A.; Sánchez, E. Application of Plasma-sprayed TiO<sub>2</sub> Coatings for Industrial (Tannery) Wastewater Treatment. *Ceram. Int.* **2015**, *41*, 14468–14474. [[CrossRef](#)]
4. Zhu, Y.; Ding, C. Characterization of Plasma Sprayed Nano-titania Coatings by Impedance Spectroscopy. *J. Eur. Ceram. Soc.* **2000**, *20*, 127–132. [[CrossRef](#)]
5. Ctibor, P.; Pala, Z.; Sedláček, J.; Štengl, V.; Píš, I.; Zahoranová, T.; Nehasil, V. Titanium Dioxide Coatings Sprayed by a Water-Stabilized Plasma Gun (WSP) with Argon and Nitrogen as the Powder Feeding Gas: Differences in Structural, Mechanical and Photocatalytic Behavior. *J. Therm. Spray Technol.* **2012**, *21*, 425–434. [[CrossRef](#)]
6. Gardon, M.; Dosta, S.; Guilemany, J.M.; Kourasi, M.; Mellor, B.; Wills, R. Improved, High Conductivity Titanium Suboxide Coated Electrodes Obtained by Atmospheric Plasma Spray. *J. Power Sources* **2013**, *238*, 430–434. [[CrossRef](#)]
7. Tomaszek, R.; Znamirovski, Z.; Pawlowski, L.; Wojnakowski, A. Temperature Behavior of Titania Field Emitters Realized by Suspension Plasma Spray. *Surf. Coat. Technol.* **2006**, *201*, 2099–2102. [[CrossRef](#)]
8. Tomaszek, R.; Znamirovski, Z.; Pawlowski, L.; Zdanowski, J. Effect of Conditioning on Field Emission of Suspension Plasma Sprayed TiO<sub>2</sub> Coatings. *Vacuum* **2007**, *81*, 1278–1282. [[CrossRef](#)]
9. Znamirovski, Z.; Ladaczek, M. Lighting Segment with Field Electron Titania Cathode Made Using Suspension Plasma Spraying. *Surf. Coat. Technol.* **2008**, *202*, 4449–4452. [[CrossRef](#)]
10. Berger, L.-M. Titanium Oxide—New Opportunities for an Established Coating Material. In Proceedings of the International Thermal Spray Conference 2003, Osaka, Japan, 10–12 May 2004; DVS Verlag: Dusseldorf, Germany, 2003.

11. Gardos, M.N. Magnéli Phases of Anion-deficient Rutile as Lubricious Oxides. Part I. Tribological Behavior of Single-crystal and Polycrystalline Rutile ( $\text{Ti}_n\text{O}_{2n-1}$ ). *Tribol. Lett.* **2000**, *8*, 6665–6678.
12. Andersson, S.; Collén, B.; Kuylenstierna, U.; Magnéli, A. Phase Analysis Studies on the Titanium-Oxygen System. *Acta Chem. Scand.* **1957**, *11*, 1641–1652. [[CrossRef](#)]
13. Mauer, G.; Gildersleeve, E.J. Using Optical Emission Spectroscopy in Atmospheric Conditions to Track the Inflight Reduction of Plasma Sprayed  $\text{TiO}_2-x$  Feedstock for Thermoelectric Applications. *Sci. Rep.* **2024**, *14*, 554–569. [[CrossRef](#)]
14. Ohmori, A.; Park, K.C.; Inuzuka, M.; Arata, Y.; Inoue, K.; Iwamoto, N. Electrical Conductivity of Plasma-Sprayed Titanium Oxide (Rutile) Coatings. *Thin Solid Films* **1991**, *201*, 1–8. [[CrossRef](#)]
15. Gardon, M.; Guilemany, J.M. A Review on Fabrication, Sensing Mechanisms and Performance of Metal Oxide Gas Sensors. *J. Mater. Sci.* **2013**, *24*, 1410–1420. [[CrossRef](#)]
16. Dervos, C.T.; Thirios, E.; Novacovich, J.; Vassiliou, P.; Skafidas, P. Permittivity Properties of Thermally Treated  $\text{TiO}_2$ . *Mater. Lett.* **2004**, *58*, 1502–1507. [[CrossRef](#)]
17. Lee, C.; Choi, H.; Lee, C.; Kim, H. Photocatalytic Properties of Nano-structured  $\text{TiO}_2$  Plasma Sprayed Coating. *Surf. Coat. Technol.* **2003**, *173*, 192–200. [[CrossRef](#)]
18. Ctibor, P.; Sedlacek, J.; Pala, Z. Dielectric and Electrochemical Properties Through-thickness Mapping on Extremely Thick Plasma Sprayed  $\text{TiO}_2$ . *Ceram. Int.* **2016**, *42*, 7183–7191. [[CrossRef](#)]
19. Agrawal, A.; Cizeron, J.; Colvin, V.L. In-Situ High Temperature TEM Observations of the Formation of Nanocrystalline TiC from Nanocrystalline Anatase ( $\text{TiO}_2$ ). *Microsc. Microanal.* **1998**, *4*, 269–277. [[CrossRef](#)] [[PubMed](#)]
20. Ctibor, P.; Hrabovský, M. Plasma Sprayed  $\text{TiO}_2$ : The Influence of Power of an Electric Supply on Particle Parameters in the Flight and Character of Sprayed Coating. *J. Europ. Ceram. Soc.* **2010**, *30*, 3131–3136. [[CrossRef](#)]
21. Ctibor, P.; Seshadri, R.C.; Henych, J.; Nehasil, V.; Pala, Z.; Kotlan, J. Photocatalytic and Electrochemical Properties of Single-layer and Multi-layer Sub-stoichiometric Titanium Oxide Coatings Prepared by Atmospheric Plasma Spraying. *J. Adv. Ceram.* **2016**, *5*, 126–136. [[CrossRef](#)]
22. Kaur, R.; Kumari, A.; Satapathy, B.R.; Gupta, A.; Kumar, S.; Chakraverty, S. Effect of Light and Electrostatic Gate at Oxide Interface  $\text{LaFeO}_3\text{-SrTiO}_3$  at Room Temperature. *Adv. Phys. Res.* **2023**, *2*, 2200087. [[CrossRef](#)]
23. Zhu, M.; Chikyow, T.; Ahmet, P.; Naruke, T.; Murakami, M.; Matsumoto, Y.; Koinuma, H. A High-resolution Transmission Electron Microscopy Investigation of the Microstructure of  $\text{TiO}_2$  Anatase Film Deposited on  $\text{LaAlO}_3$  and  $\text{SrTiO}_3$  Substrates by Laser Ablation. *Thin Solid Film.* **2003**, *441*, 140–144. [[CrossRef](#)]
24. Matweb. Available online: [www.matweb.com](http://www.matweb.com) (accessed on 15 January 2024).
25. Ismael, M.; Wark, M. Perovskite-type  $\text{LaFeO}_3$ : Photoelectrochemical Properties and Photocatalytic Degradation of Organic Pollutants Under Visible Light Irradiation. *Catalysts* **2019**, *9*, 342. [[CrossRef](#)]
26. Takeuchi, T.; Tabuchi, M.; Kageyama, H. Preparation of Dense  $\text{BaTiO}_3$  Ceramics with Submicrometer Grains by Spark Plasma Sintering. *J. Am. Ceram. Soc.* **1999**, *82*, 939–943. [[CrossRef](#)]
27. Mikkenie, R. Materials Development for Commercial Multilayer Ceramic Capacitors. Ph.D. Thesis, University of Twente, Enschede, The Netherlands, 2011.
28. Masingboon, C.; Eknapakul, T.; Suwanwong, S.; Buaphet, P.; Nakajima, H.; Mo, S.-K.; Thongbai, P.; King, P.D.C.; Maensiri, S.; Meevasana, W. Anomalous Change in Dielectric Constant of  $\text{CaCu}_3\text{Ti}_4\text{O}_{12}$  Under Violet-to-Ultraviolet Irradiation. *Appl. Phys. Lett.* **2013**, *102*, 202903. [[CrossRef](#)]
29. Bertrand, G.; Berger-Keller, N.; Meunier, C.; Coddet, C. Evaluation of Metastable Phase and Microhardness on Plasma Sprayed Titania Coatings. *Surf. Coat. Technol.* **2006**, *200*, 5013–5019. [[CrossRef](#)]
30. Cizek, J.; Dlouhy, I.; Siska, F.; Khor, K.A. Modification of Plasma-sprayed  $\text{TiO}_2$  Coatings Characteristics via Controlling the In-flight Temperature and Velocity of the Powder Particles. *J. Therm. Spray Technol.* **2014**, *23*, 1339–1349. [[CrossRef](#)]

**Disclaimer/Publisher’s Note:** The statements, opinions and data contained in all publications are solely those of the individual author(s) and contributor(s) and not of MDPI and/or the editor(s). MDPI and/or the editor(s) disclaim responsibility for any injury to people or property resulting from any ideas, methods, instructions or products referred to in the content.